The NTSC VLBI System and its application in UT1 measurement

Dang Yao (姚当)[1,2], Yuan-Wei Wu (吴元伟)[1], Bo Zhang (张波)[3], Jing Sun (孙靖)[4] , Yan Sun (孙焱)[2,3], Shuang-Jing Xu (徐双敬)[3], Jia Liu (刘佳)[1], Lang-Ming Ma (马浪明)[1], Jian-Jun Gong (弓剑军)[1], Ying Yang (杨颖)[1] and Xu-Hai Yang (杨旭海)[1]

[1] National Time Service Center, Chinese Academy of Sciences, Xi'an 710600, China; *yaodang@ntsc.ac.cn, yuanwei.wu@ntsc.ac.cn*

[2] University of Chinese Academy of Sciences, Beijing 100049, China

[3] Shanghai Astronomical Observatory, Chinese Academy of Sciences, Shanghai 200030, China

[4] National Astronomical Observatories, Chinese Academy of Sciences, Beijing 100101, China

Abstract In order to measure the Universal Time (UT1) in real time, National Time Service Center (NTSC) has built a VGOS-like (VLBI Global Observing System) broadband VLBI network, which includes three 13-m radio telescopes located in Jilin, Sanya and Kashi, and a data analysis center in Xi'an. Each station is equipped with a highly stable hydrogen atomic clock and a self-developed VLBI backend, and is co-located with two GPS receivers. This VGOS-like VLBI network may play an important role in improving the Chinese broadband VLBI technology and making valuable contributions to domestic VLBI measurements of UT1. In this paper, we introduce the specifications of this VLBI network, and present the UT1 measurements at C-band conducted in 2018 using the Jilin-Kashi baseline of this network. The comparisons between our UT1 estimates and those provided by IERS suggest that the NTSC VLBI network is capable to determine UT1 accurate at the level of 58.8 µs.

Key words: instrumentation: interferometers — methods: observational — time — Earth

1 INTRODUCTION

Earth orientation parameters (EOP), including Universal Time (UT1), polar motion (PMX, PMY), and corrections of the conventional Precession/Nutation model ($d\psi$, $d\varepsilon$), are a collection of parameters that provide the rotation between the International Terrestrial Reference Frame (ITRF) and the International Celestial Reference Frame (ICRF). Thus, EOP are widely used in Astronomy, Geosciences, Navigation, Deep Space Tracking and Precise Orbit Determination. Among the five parameters of EOP, UT1, the measurement of rotation angle of the Earth, is the most unpredictable parameter that irregularly changes day by day, therefore needs daily observations. The International VLBI Service for Geodesy and Astrometry (IVS) organizes two modes of observations to measure the EOP. The regular mode (R1, R4) is 24 h experiment with ∼10 stations, observed twice a week with

UT1 accuracy of about 7 µs and a latency of 1–2 weeks (Schuh et al. 2010). The intensive mode (INT1, INT2 and INT3) observes one hour per day using 2–4 stations, with a typical accuracy of about 15 µs and a latency of less than one day (Böhm et al. 2012).

In order to achieve a better accuracy, continuous data flow, and short latency of EOP products, in 2000s, IVS formed the VLBI2010 Committee and the Implementation Team to define and design the next-generation VLBI system, i.e., the VLBI2010 system. The next-generation geodetic VLBI network is finally named as the VLBI Global Observing System (VGOS). It is characterized by a high temporal resolution of the observations by using fast slewing antennas and a broad radio frequency bandwidth, with the aim of achieving the accuracy of 1 mm station position and 0.1 mm yr^{-1} velocity on global scales, continuous observing (7 d per week and 24 h per day), and posting of initial geodetic results within 24 h after observations

Table 1 The Geographic Coordinate of the Three NTSC VLBI Antennas

Site	Station code	Longitude	Latitude	Above sea level
Jilin station	JL	126°	43°	313 m
Kashi station	KS	76°	39°	1242 m
Sanya station	SY	109°	18°	12 m

(Niel et al. 2005). As of 2018, there are 22 VGOS projects with 24 new radio telescopes already built or under construction.

National Time Service Center (NTSC)[1] of Chinese Academy of Sciences (CAS) started to build a VGOS-like broadband VLBI system since 2013. It consists of three 13-m diameter telescopes with baseline lengths ranging from 3000 km to 4000 km (Fig. 1) and a data analysis center. The construction was finished in 2016. Following a period of commissioning and debugging, the first fringes for the radio source 3C84 and an artificial GEO (Geostationary Earth Orbit) satellite were successfully detected in the middle of 2016. Nowadays this VLBI system has been used for artificial satellite orbit determination (Gong et al. 2018) and UT1 measurement.

In this paper, we introduce the NTSC VLBI system in Section 2, and UT1 experiments in the intensive mode conducted in 2018 are presented in Section 3. Analysis and results of the experiments are shown in Section 4. Finally, the conclusion and future plans are summarized in Section 5.

2 NTSC VLBI SYSTEM

2.1 Imaging Capability

The geographic coordinates of Jilin, Kashi and Sanya stations are listed in Table 1. It is noted that the Sanya station has the ability to observe most of the southern sky sources ($\sigma \geq -70°$). The Jilin-Kashi baseline, which is the longest east-west baseline, may play an important role in domestic UT1 measurement.

The NTSC VLBI array can also carry out astrometric and astrophysical observations which require properly calibrated visibility amplitudes and phases. In the top panels of Figure 2, we show the simulated u-v coverage of the sources at different declinations. The NTSC network has a common view of $\sim$7 h for a source at Dec $= -20°$, $\sim$11 h for a source at Dec $= 20°$, and $\sim$16 h for a source at Dec $= 60°$. It can be seen that the u-v coverage of the NTSC VLBI network is sparse, especially, there is a hole

due to the lacking of short baseline, which means a limited imaging capability.

In the bottom panels of Figure 2, we show the simulated u-v coverage by combing the Chinese VLBI Network (CVN, Zheng 2015) and the NTSC array, both of them cover the S/X band. The blue tracks are the baselines among KUNMING, URUMQI, MIYUN and SESHAN25, the red u-v tracks are the baselines increased by the three NTSC stations. It can be seen that the longest baseline is increased from $\sim$3000 km to $\sim$4000 km, this means an improvement of the synthetic beam by 30%. Meanwhile, the combination of the two networks also increases the short baselines, which is essential for study of sources with extended structure, for example the radio jet of M87 (Walker et al. 2018).

2.2 Antenna and Receiver System

The three 13-m antennas were designed and constructed by the 39th Institute of China Electronics Technology Group Corporation (CETC). The quasi-parabolic mirror of the radio telescope has a diameter of 13 m and stands $\sim$17 m above the ground. The secondary quasi-hyperbolic mirror was fixed by the quadrapod support structure with diameter of 1.48 m (see Fig. 3).

The maximal slewing rate of antenna is $12°$ s^{-1} in azimuth and $6°$ s^{-1} in elevation, and the minimal slewing rate is $0.002°$ s^{-1}, which makes it be able to track not only radio sources but also near-earth satellites. The antenna can rotate clockwise and counterclockwise $270°$ relative to the south direction in azimuth and from $5°$ to $90°$ in elevation. By observations of ICRF radio sources (with position accuracy of $\sim$1 mas) and building a 18-parameter modified model, the pointing accuracy is achieved at the level of 30 arcseconds (Wu et al. 2020). The detail information of the antenna system is summarized in Table 2.

Cryogenic Cooling broad-band receivers were designed and produced by the 16th Institute of CECT. The frequency ranges from 1.2 to 9 GHz for Jilin and Sanya. For Kashi station, due to strong, up to 200 kilowatt, radio frequency interference (RFI) from a nearby meteorologic radar at 5.43 GHz, the frequency band over 5 GHz are temporary filtered out. Thus, Kashi station is currently only available from 1.2 to 5 GHz. The receivers can receive right- and left-hand circular polarization (RCP and LCP) signals simultaneously.

The cryogenic system cools the low noise amplify (LNA) down to $\sim 10 - 20$ K, the noise temperature of the receiver is about 50 K. However, the typical system temperature measured at 5 GHz towards the zenith direction
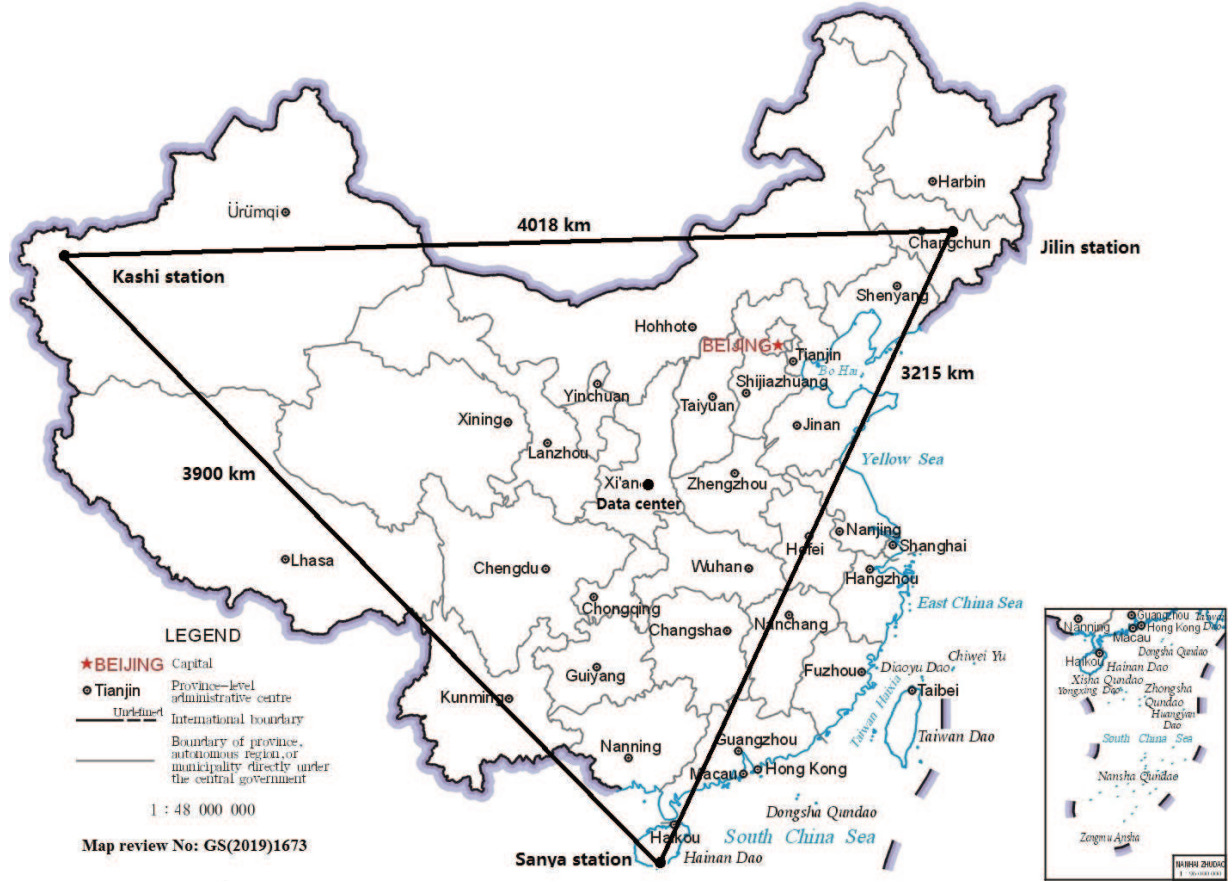
Fig. 1 The geographical distribution of the NTSC VLBI network consists of three stations located in Jilin, Sanya and Kashi. The data analysis center is in Xi'an.

Table 2 Specifications of NTSC VLBI Antennas

Parameter	Value
Antenna mount	Altazimuth
Reflector configuration	Cassegrain
Main dish Diameter	13 m paraboloid
Main dish Surface accuracy	0.3 mm rms
Secondary refl. Diameter	1.48 m
Secondary refl. Surface accuracy	0.1 mm rms
Pointing accuracy	30 as
Frequency range	1.2∼9 GHz
Azimuth range[a]	$-270° \sim +270°$
Elevation range	$5° \sim 92°$
Azimuth slewing rate	$12°\,\mathrm{s}^{-1}$
Elevation slewing rate	$6°\,\mathrm{s}^{-1}$
Azimuth/Elevation slewing accel.	$3°\,\mathrm{s}^{-2}$
Minimal slewing rate	$0.002°\,\mathrm{s}^{-1}$

[a] The south is 0°.

are 70 K, 75 K and 65 K for Sanya, Kashi and Jilin stations, respectively, due to the various atmospheric noise, ground radiation noise, RFI, etc.

The sensitivity of the antenna system is generally characterized by the System Equivalent Flux Density (SEFD), that can be determined by,

$$\mathrm{SEFD} = \frac{2 \times k \times T_{\mathrm{sys}}}{A \times \eta \times 10^{-26}}, \tag{1}$$

k is Boltzmann's constant ($1.38 \times 10^{-23}\,\mathrm{m^2\,kgs^{-2}\,K^{-1}}$), A is the aperture area of antenna (m²), and η is the aperture efficiency, which is 0.55 for NTSC antennas. The SEFDs of the three stations are 2647, 2836 and 2457 Jy, respectively. At current stage, the elevation dependency of the SEFD has not been considered yet.

2.3 VLBI Backend and Data Acquisition System

Apart from the 13-m antennas and the cryogenic cooling broad-band receiver, each station is equipped with a VLBI digital backend, a hydrogen clock with the stability of 5×10^{-13} @ 1 s and 5×10^{-16} @ 1 d, a weather station and two GNSS receivers (One for geodetic use, the other for time synchronization).

The over-view of the signal chain is shown in Figure 4. The system temperature calibration (TCAL) and phase calibration (PCAL) block, developed by Shanghai
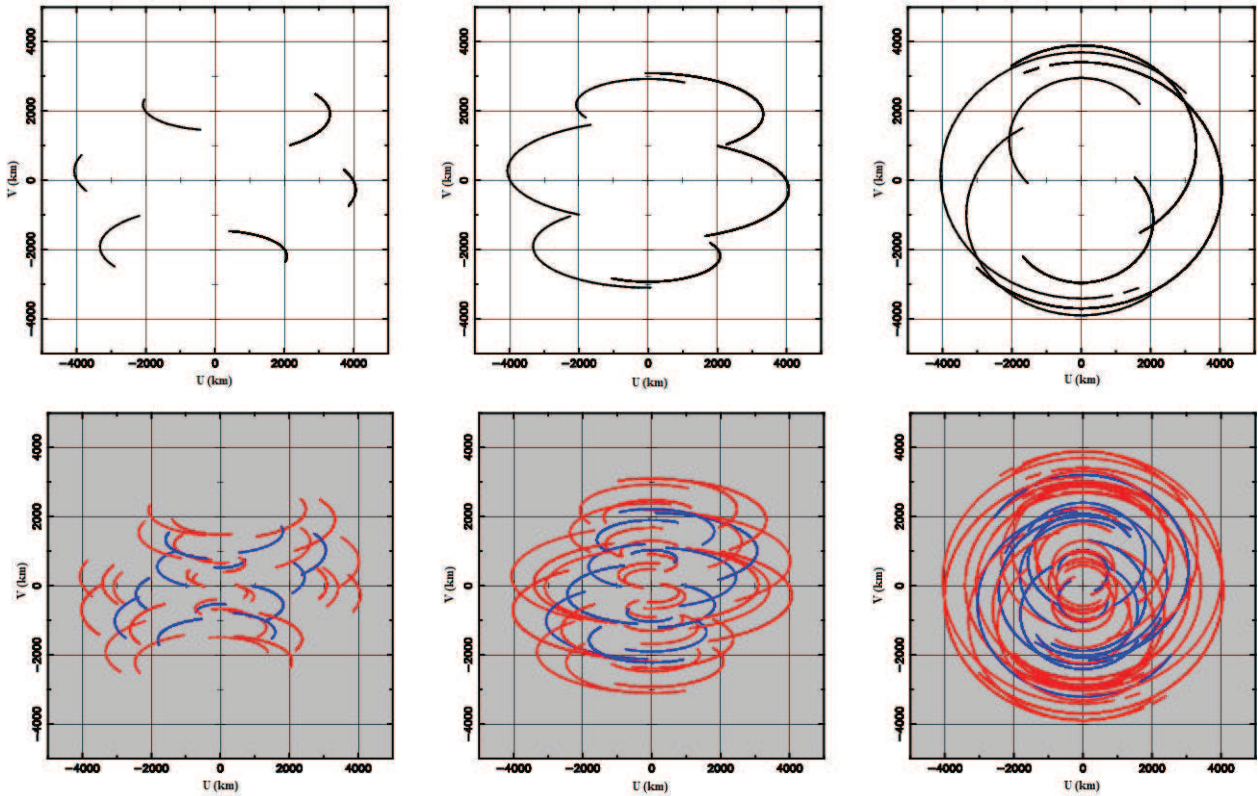
Fig. 2 The top panels are the simulated u-v coverage with the NTSC VLBI array for the source at declination: $-20°$ (*left*), $20°$ (*middle*), and $60°$ (*right*), respectively. The bottom panels are the simulated u-v coverage with the seven Chinese VLBI antennas for the source at declination: $-20°$ (*left*), $20°$ (*middle*), and $60°$ (*right*), respectively.

**Fig. 3** The 13-m Cassegrain radio telescope at Jilin station.

Astronomical Observatory (SHAO), allows for injecting a tone generator of 5 MHz PCAL signal into the signal path at the feedhorn, which is essential to remove instrumental phase differences raised by the receiver and the samplers. The TCAL signal is used to measure the system temperature. As the powers of satellite signals are much stronger than that of radio sources, after the first LNA (30 dB of

gain), an optional electronic switch is added to change the signal chain between the quasar and satellite path to avoid saturation of the second LNA (40 dB of gain).

The down-convert (DC, 30 dB of gain) selects broadband signals with local oscillators, phase-locked to a 10 MHz tone from the hydrogen clock, and produces six intermediate frequency (IF) signals: 1) RCP/LCP 50–
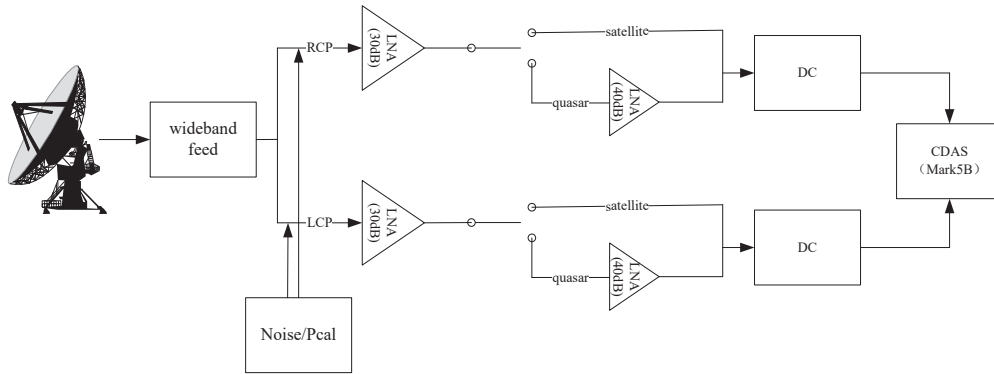
Fig. 4 Diagram of the signal chain from the feed to the receiver with two LNA to the IF signal outputs from DC to the VLBI recorder.

Table 3 Specifications of VLBI Digital Backend CDAS

Parameter	Value
Max IF input number	2
Polarization	RCP/LCP
Frequency range	50–1024 MHz
	512–1024 MHz
	50–1024 MHz
Max channel	32
Each channel band	32 MHz (2-bit sample)
	64 MHz (1-bit sample)
Max sampling rate	2 Gbps
Sampling bit	1/2-bit
Max data rate	4×2 Gbps
Out data format	Mark5B

512 MHz; 2) RCP/LCP 512–1024 MHz; 3) RCP/LCP 50–1024 MHz.

Data digitization and formatting are processed by the Chinese VLBI Data Acquisition System (CDAS, developed by SHAO, Zhu et al. 2011), which is synchronized to the hydrogen clock through 1 pulse-per-second (1PPS) signal. The input signal from DC output is split into two paths in CDAS. One path is to an analog monitoring device that records and displays the channel power on CDAS control software, the other one is to A/D sampler, that digitizes analog signals into 1-bit 50–1024 MHz data streams, or 2-bit 50–512 MHz/512–1024 MHz data streams. The maximal sampling rate is 1024 mega-sample per-second with 2-bit digitization, resulting a 2 Gbps data rate at 512 MHz bandwidth. The CDAS can maximally support 4×512 MHz band-width and 8 Gbps data rate (Table 3).

After the sampling, the data stream from CDAS is then sent to a record server through fiber-optics, and saved as the Mark5B data format. The record sever is equipped with Redundant Arrays of Independent Drives (RAID) file system, which allows flexible data recording and data transporting.

2.4 Operations

In order to effectively manage the NTSC VLBI array, all three antennas are designed to be remotely controlled via the internet. Remote observations can be carried out in the operation room located in Xi'an. Meanwhile, each site has an observing assistant who is responsible for maintaining the equipment and carrying out on-site observations in case of internet interruption.

The schedule file (VEX file) is produced by the Vienna VLBI and Satellite Software (VieVS, Sun et al. 2014). It can be used in manual mode, where the user explicitly specifies all or part of the information required for schedule, or in automatic mode. For the observations shown in this paper, the automatic mode is used. The VEX file is then transferred to each site via the internet. During the observation, the Station Control Software (SCS) on each site reads in the vex file, then controls and monitors all corresponding on-site devices. Observational information including the azimuths and elevations of antenna, the parameter setup of DC, the CDAS status, etc., is collected by the SCS and saved in a log file for further analysis and fault finding. Before the UT1 observation, usually, a fringe checking on a strong calibrator is carried out to make sure that the system is working properly.

3 UT1 EXPERIMENTS

Traditionally, geodetic VLBI experiments are conducted at S-band (2.2–2.3 GHz) and X-band (8.2–8.6 GHz), while, due to the strong RFI at Kashi station, currently, we adopted 4.4 to 4.9 GHz (512 MHz, RCP signal and 2 Gbps) bandwidth for UT1 test experiments. The C-band sources, used for the experiments, are compiled from the rfc_2018c catalogue of compact radio sources[2] (Fig. 5).

---

[2] *http://alt.astrogeo.org/rfc/*
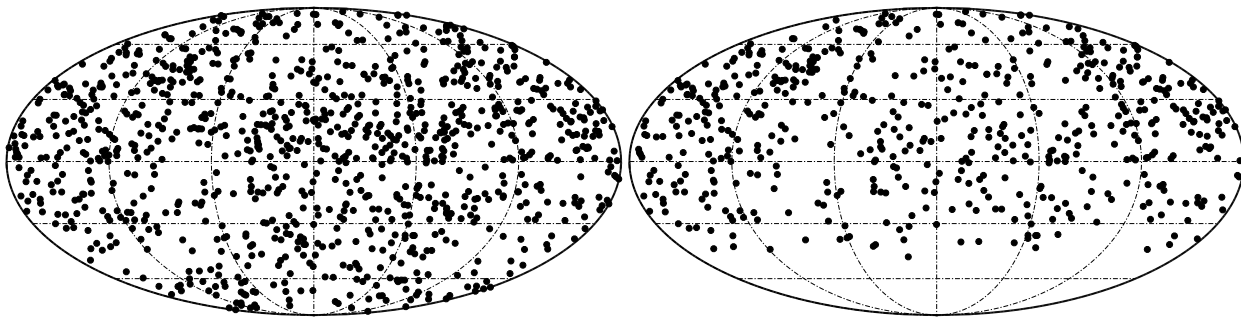
Fig. 5 The distribution of candidate sources for UT1 experiment. The IVS candidate sources at S/X-band are shown in the left panel. The NTSC candidate sources at C-band are shown in the right panel, which are selected from rfc_2018c.

The number of sources of our C-band source list is about half of the IVS S/X catalogue.

From June to December of 2018, in total, we carried out 113 UT1 experiments. During July, August, and September, more than one (two to five) sessions were observed within one day.

With the aim to detect stable fringes, we used several constrains listed below to select sources.

– The cut-off elevation angle of $20°$,
– The minimum source flux is $0.6\,\mathrm{Jy}$,
– The scan duration is limited in 60–$200\,\mathrm{s}$,
– The minimum SNR of 15 at C-band.

This results in a mean scan number of 36 for each 1-hour session, as shown in Figure 6 and the mean number of sources is 21.

In addition, we scheduled two half hour strong source blocks before and after the UT1 block (Fig. 7) to monitor the stabilities of hydrogen clocks and to estimate and correct the residual clock drifts. As we found long-term clock and/or instrumental instabilities occasionally. For instance, in Figure 8, it can be seen a change of clock rate at $\sim$14:00 of 2018 July 25.

4 DATA ANALYSIS AND RESULTS

4.1 Correlation and Post-correlation

The Mark5B raw data from each station are sent to the correlator center by mail for processing, while the small mount (10–30 s) of fringe checking data is transferred via the internet. The flow diagram of data processing is shown in Figure 9. The DiFX software (Deller et al. 2007) correlator is used for correlation. It replays the observed data from stations, compensates for the changing phase difference by fringe rotation, then the time-series data is converted into frequency-series data (channelized) prior to cross multiplication. The DiFX software installed in NTSC correlator center is consist of a 20-node cluster with a 200 TB storage space. After correlation, the data are saved as FITS and MK4 format files for further analysis.

The visibility data are processed using a ParselTongue (Kettenis et al. 2006) pipeline script developed by the NTSC VLBI team, the pipeline reduce the FITS file by call the NRAO Astronomical Image Processing System (AIPS) to determine the residual delay and then calculates the total baseline delay: (1) loading and editing of raw uv data, (2) ionospheric delay calibration, (3) clock drift and manual phase calibration to correct residual equipment delays, (4) bandwidth synthesis to determine the residual baseline delay, (5) calculating the total ionospheric-free baseline delays.

Shown in Figure 10 is an example of the residual Multi-Band Delay (MBD). The residual MBD in most UT1 sessions is in range from –0.2 to 0.2 ns. The two half-hour blocks at the beginning and the end (7.0–7.5 h and 8.5–9.0 h) are the two strong-source blocks, and the scans within 7.5 and 8.5 h form the 1-hour UT1 block.

4.2 Estimation of UT1-UTC

We estimated UT1-UTC by using the VieVS. The observed ionospheric-free total delay from ParselTongue output and the meteorological data (temperature, humidity and atmosphere pressure) collected by the weather stations are combined to generate the ASC II code files developed by US National Geodetic Survey (NGS), which are the inputs for the VieVS.

For propagation delays, we only consider the troposphere influence, as the ionospheric delay is already compensated based on the International GNSS Service (IGS) global model of TEC maps by using the AIPS Task TECOR. The station coordinates were fixed to apriori positions measured by GPS local survey. Regarding station coordinate correction, we adopt the Conventions 2010 provided by International Earth Rotation and Reference
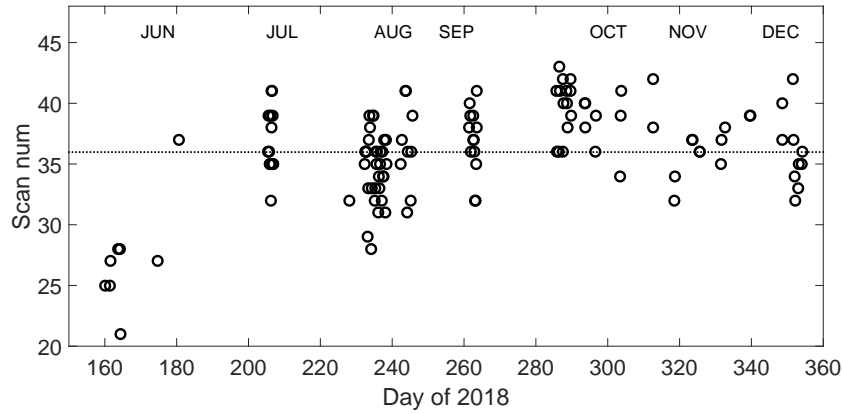
Fig. 6 The scan number of sessions in 2018. The *dot line* indicates the average scan number of 36.
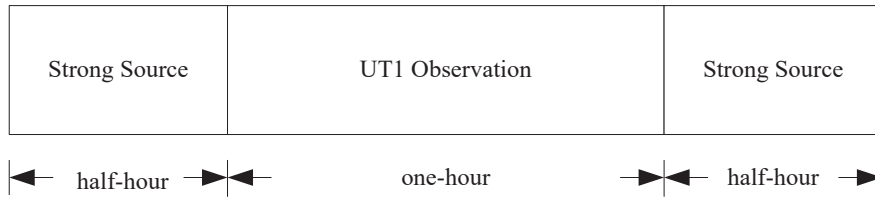
**Fig. 7** Diagram of the 2 h UT1 sessions.
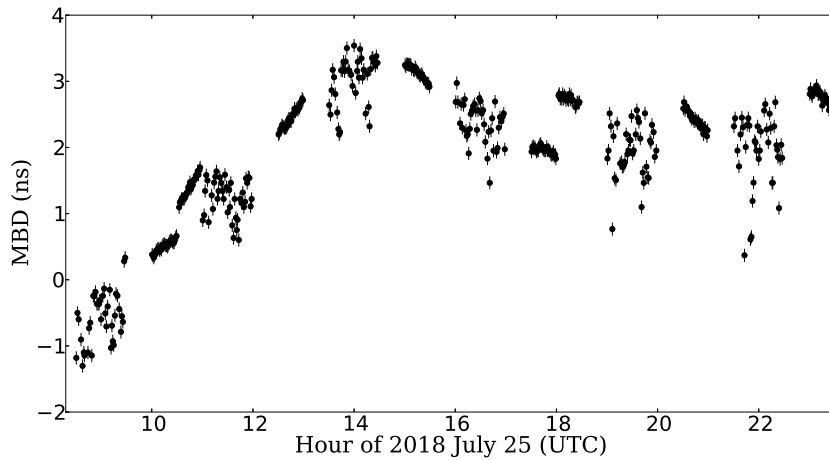
Fig. 8 The residual multi-band delay (MBD) of 2018 July 25. The *dense concentrated points* denote the MBD of strong source blocks and the *scattered points* denote the MBD of UT1 blocks.

Systems Service (IERS) (Petit & Luzum 2010), that including solid earth tides, tidal ocean loading (FES2004), pole tide and ocean pole tide, while the non-tide atmospheric loading was not taken into account. For the priori EOP, the IERS C04 14 (here after C04 14) was used and the high frequency (diurnal and subdiurnal) corrections were compensated in polar motion and UT1. The Global Mapping Function (GMF) for tropospheric delay was used for the UT1 test experiment (Kareinen et al. 2015). Jilin station was chosen as the reference station in the analysis. The detailed parameterization can be seen in Table 4.

Then the observation delays and the theoretical delays computed by VieVS were entrance to the least-squares adjustment to determine the best value of the estimated quantities, including the clock offsets, zenith wet tropospheric delay (ZWD) offsets and UT1 offsets [3].

The 113 UT1 sessions are analyzed by the VieVS, it eliminates outlier delay values, i.e., the scan with residuals larger than 10 cm. Finally, we get the UT1-UTC estimations for 107 sessions. There are six sessions for which we

---

[3] The corrections to polar motion and Precession/Nutation were not estimated due to the limited scan number in one hour observation.
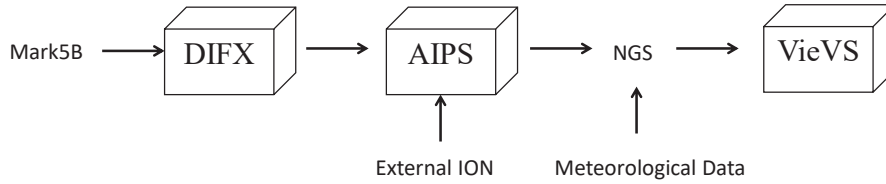
Fig. 9 Flowchart of the data analysis. The Mark5B data is correlated by the DiFX, the post-correlation is performed by AIPS, finally, the VieVS is used to estimate the parameter.
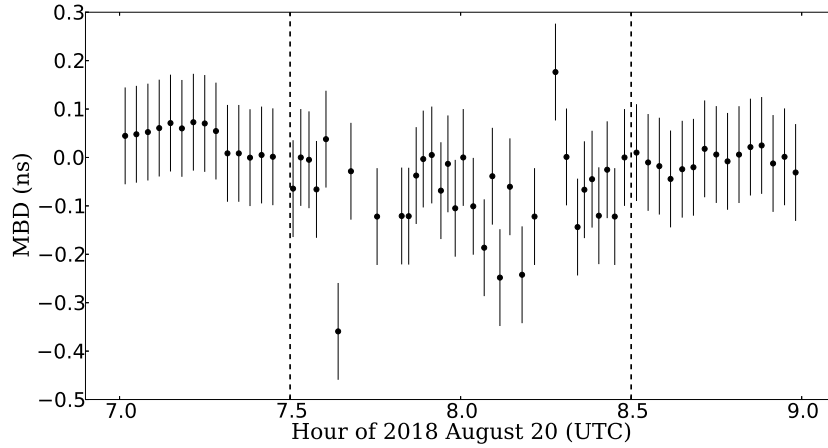
Fig. 10 The example of the residual MBD resolved by AIPS. The error bar denotes a typical delay uncertainty of 0.1 ns. The two perpendicular *dashed lines* are the borderline between the UT1 block and strong calibrator blocks.
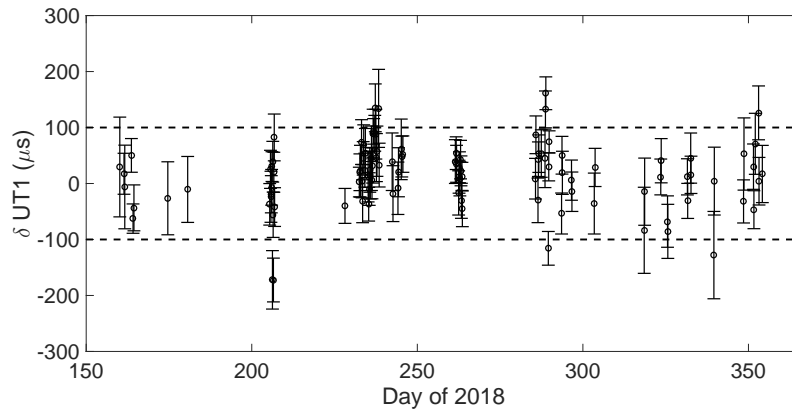

Fig. 11 Differences between UT1-UTC obtained from NTSC observations and C04 14 series from June to December in 2018. Around 96% of the points are within ± 100 μs (denoted by the *horizontal dashed lines*).

Table 4 The Analyzed Parameters in UT1 Determination

Parameter	Value	Parameter	Value
Observation type	Group delay	Precession/Nutation	IAU[a] 2006 model
Solution type	One standalone	TRP MF	GMF
Elevation cut off	20°	dUT1 estimated interval, constraint	1440 min, 0.0001
Ephemerides	DE 421 ephemeris	ZWD estimated interval, constraint	flexible, 1.5 cm
A priori EOP	EOP C04 14	Clock estimated interval, constraint	flexible, no const.
High frequency EOP	IERS Conventions 2010	Reference station	Jilin
Source coordinate	ICRF2	Station position	ITRF (GPS local survey)

[a] International Astronomical Union
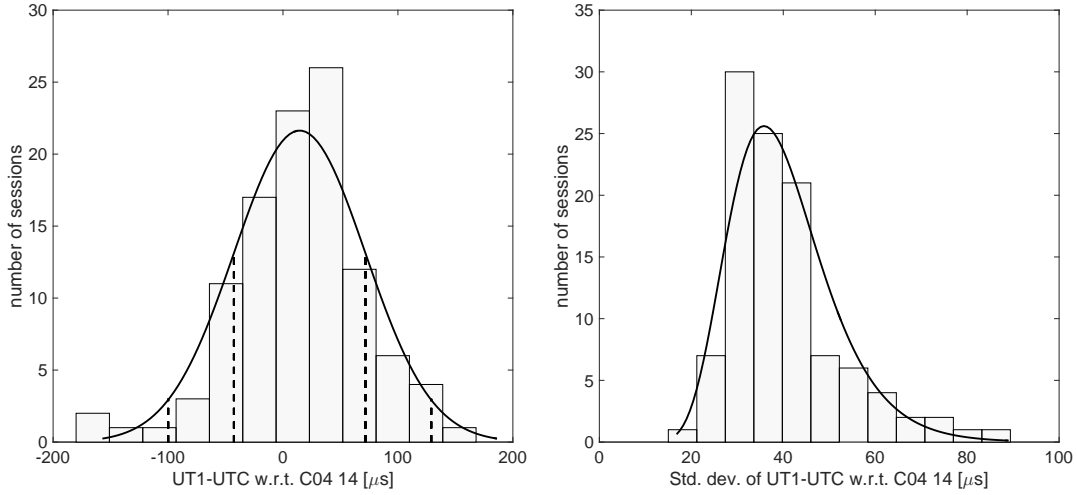
Fig. 12 Distribution of differences and their formal errors in UT1-UTC between NTSC VLBI and C04 14 from June to December in 2018. The left panel is the distribution UT1-UTC differences w.r.t. C04 14. The right panel is the distribution of the formal errors. The *dashed lines* in the left panel indicate the 1-sigma (–42.7 to 71.7 µs) and 2-sigma (–99.9 to 128.9 µs) confidence intervals. The theoretical curves for a Gaussian distribution (left) and an empirical chi-distribution (right) are overlaid.

cannot estimate the UT1-UTC due to the equipment troubles (e.g., the losing lock of hydrogen clock and breakdown of the record server).

In general, if random noises were the only error source, then the χ^2 of session would be $\sim$1. In reality, we find that the χ^2 of most sessions are in 3–7 in NTSC UT1 experiments, indicating the presence of other error sources and/or modeling errors, for instance, the errors in station coordinates, which require further detailed investigation.

4.3 UT1 Comparison

In this subsection, we evaluate the accuracy of UT1 experiments by comparing our estimation with C04 14 and IVS INT1 results. Figure 11 shows the differences between our measurement and C04 14. Such differences can be an indicator of the agreement between our measurement and the true value (accuracy). The histogram of these differences is shown in the left panel of Figure 12, which follows a Gaussian distribution. On average, there is 14.5 µs bias between our estimation and C04 14, and the full width at half maximum (FWHM) is 114.4 µs (2σ).

The 14.5 µs bias of our results may be partly due to bias of our station coordinates, and partly due to the station clock offsets, as studied by Hobiger et al. (2009), that the VLBI reference station clock offsets can result in a bias of UT1 estimates, and partly due to unknown absolute electronics delays. As pointed by Anderson et al. (2018), the full-time offset between the reception of a wavefront by a VLBI antenna, and the propagation of that wavefront through the receiver electronics, backend electronics, and

Table 5 The Comparison in the UT1-UTC Estimation of NTSC and IVS INT1 Results w.r.t. the C04 14

Type	RMS(µs)	$< \delta$UT1$>$(µs)	$<$formal error$>$(µs)
NTSC measured	58.8	14.5	40.3
IVS INT1	25.5	6.9	11.6

associated cables, and the association of a time tag is not known in VLBI. Further, the absolute offset between VLBI time and Coordinated Universal Time (UTC) is not known (Himwich 2003; Himwich 2005; Himwich et al. 2017; Anderson et al. 2018). Such bias can only be reduced by further international and domestic VLBI sessions.

The error bars in Figure 11 are the formal errors of the least-square fitting, which indicates the repeatability of the measurement (precision), the histogram of which is shown in the right panel of Figure 12. Regarding the repeatability, roughly 82% of sessions give formal errors for UT1-UTC for less than 40 µs, following the chi-square distribution.

Further, we compare the accuracy and precision of the NTSC measurement and IVS INT1 result in 2015–2018. In Table 5, listed are the Root-Mean-Square (RMS), the average values of the difference w.r.t. the C04 14 and the formal error. It can be concluded that the UT1-UTC accuracy achieved with the Jilin-Kashi baseline is on average 2–3 times larger than the IVS INT1. Taking into account the baseline length, the system reliability and the observing frequency, the accuracy currently achieved is reasonable.

5 SUMMARY AND FUTURE PLAN

We have constructed, commissioned and are now operating three new 13-m radio telescopes for geodetic VLBI at Jilin, Kashi and Sanya of China. From June to December, the last half year of 2018, we conducted 113 times UT1 experiments.

In this paper, we presented results of these experiments. By statistics, a bias of 14.5 μs is found between our estimation and C04 14, and the RMS of UT1-UTC differences w.r.t. C04 14 is 58.8 μs. The repeatability of the UT1 experiments is about 40 μs, which is around 3 times larger than the IVS INT1 results. Overall, those results indicate the VLBI network is capable to determine UT1.

Regarding the UT1 uncertainty, the inaccurate station position might be one of the primary error sources, we will join the domestic and international 24 h geodetic VLBI campaigns to improve the position accuracy. In addition, optimized source selection and scheduling would be helpful to reduce the systematic error. We also identified several problems with station equipment, which will be solved in the near future. The serious RFI at the KS station can be overcome by adding a filter to save the observing frequency at 8–9 GHz. Finally, we look forward to making contributions to domestic VLBI measurements of EOP, especially the UT1.

References

Anderson, J. M., Beyerle, G., Glaser, S., et al. 2018, J. Geod, 92, 1023

Böhm, J., Böhm, S., Nilsson, T., et al. 2012, Geodesy for Planet Earth, 136, 1007

Deller, A. T., Tingay, S. J., Bailes, M., & West, C. 2007, PASP, 119, 318

Gong, J. J., Ma, L. M., Yao, D., et al. 2018, Journal of Time and Frequency, 4, 354 (in Chinese)

Himwich, E. 2003, 2002 Annual Report of the IVS, *ftp://ivscc.gsfc.nasa.gov/pub/annual-report/2002/pdf/ivs-nc.pdf*

Himwich, E. 2005, 2004 Annual Report of the IVS, *ftp://ivscc.gsfc.nasa.gov/pub/annual-report/2004/pdf/ivs-nc.pdf*

Himwich, E., Bertarini, A., Corey, B., et al. 2017, the 23rd Working Meeting of the European VLBI Group for Geodesy and Astrometry (EVGA), 172, *http://www.oso.chalmers.se/evga/23_EVGA_2017_Gothenburg.pdf*

Hobiger, T., Koyama, Y., Boehm, J., et al. 2009, Advances in Space Research, 43, 910

Kareinen, N., Hobiger, T., & Haas, R. 2015, Earth, Planets and Space, 67, 181

Kettenis, M., van Langevelde, H. J., Reynolds, C., & Cotton, B. 2006, in ASPC, Astronomical Data Analysis Software and Systems XV, 351, (eds.) Gabriel, C., Arviset, C., Ponz, D., & Enrique, S., 497

Niel, A., Whitney, A., Petrachenko, W., et al. 2005, IVS WG3 Report, *http://ivscc.gsfc.nasa.gov/about/wg/wg3*

Petit, G.,& Luzum, B. 2010, IERS Technical Note No. 36

Schuh, H., Böhm, J., Englich, S., et al. 2010, IVS 2010 General Meeting Proceedings, 251

Sun, J., Böhm, J., Nilsson, T., et al. 2014, J. Geod, 88, 449, *https://doi.org/10.1007/s00190-014-0697-9*

Walker, R. C., Hardee, P. E., et al. 2018, ApJ, 855, 128

Wu, W.-Y., Ma, L.-M., Yao, D., et al. 2020, Journal of Time and Frequency, 43, 41 (in Chinese), *https://kns.cnki.net/KCMS/detail/61.1405.p.20200511.1657.004.html*

Zheng, W. M. 2015, IAA General Assembly, Meeting 22, 2255896

Zhu, R. J., Zhang, X. Z., & Wei, W. R. 2011, Progress in Astronomy, 29, 207